ARTICLES
https://doi.org/10.1038/s41563-022-01360-9
nature materials

Nanoparticle-modified microrobots for in vivo antibiotic delivery to treat acute bacterial pneumonia

Fangyu Zhang[1,3], Jia Zhuang[1,3], Zhengxing Li[1,3], Hua Gong[1,3], Berta Esteban-Fernández de Ávila[1], Yaou Duan[1], Qiangzhe Zhang[1], Jiarong Zhou[1], Lu Yin[1], Emil Karshalev[1], Weiwei Gao[1], Victor Nizet[2], Ronnie H. Fang[1], Liangfang Zhang[1]✉ and Joseph Wang[1]✉

Bioinspired microrobots capable of actively moving in biological fluids have attracted considerable attention for biomedical applications because of their unique dynamic features that are otherwise difficult to achieve by their static counterparts. Here we use click chemistry to attach antibiotic-loaded neutrophil membrane-coated polymeric nanoparticles to natural microalgae, thus creating hybrid microrobots for the active delivery of antibiotics in the lungs in vivo. The microrobots show fast speed (>110 μm s^{-1}) in simulated lung fluid and uniform distribution into deep lung tissues, low clearance by alveolar macrophages and superb tissue retention time (>2 days) after intratracheal administration to test animals. In a mouse model of acute *Pseudomonas aeruginosa* pneumonia, the microrobots effectively reduce bacterial burden and substantially lessen animal mortality, with negligible toxicity. Overall, these findings highlight the attractive functions of algae–nanoparticle hybrid microrobots for the active in vivo delivery of therapeutics to the lungs in intensive care unit settings.

The potential of micro-/nanorobots for biomedical applications has been extensively explored over the last decade[1–3]. Although early microrobot designs, consisting primarily of rigid metallic or polymeric structures, allowed for various in vitro applications, novel platforms based on biocompatible and deformable materials have offered some unique advantages towards in vivo operations, including improved drug delivery, deep-tissue imaging and precision microsurgery[4–6]. The in vivo application of these microrobots has typically been restricted due to limitations in the availability of natural fuels, accessibility to certain organs and tissues, and potential toxicity. Biodegradable zinc- and magnesium-based microrobots have been used for drug delivery in the gastrointestinal tract[7,8]. Magnetically powered microrobots have demonstrated deep penetration in the vitreous humour[6] and actuation in the peritoneal cavity[9,10]. Achieving active propulsion in other body locations is difficult, but if successful, would offer unprecedented benefits for the treatment of important diseases.

Here we report a bioinspired microrobot platform consisting of nanoparticle (NP)-modified algae for active therapeutic delivery to treat lung disease. Biohybrid microrobots, which combine the motility of natural organisms with the multifunctionality of synthetic components, have recently been studied as an alternative to purely synthetic microrobots[11,12]. For instance, *Magnetococcus marinus*, which swims along local magnetic fields and towards low oxygen concentrations, were used for transporting drugs into hypoxic tumour regions[13]. The natural movement of sperm has been leveraged to construct hybrid microrobots with distinct advantages towards assisted fertilization[14]. In our design, we create a biohybrid microrobot consisting of *Chlamydomonas reinhardtii* microalgae modified with neutrophil membrane-coated and drug-loaded polymeric nanoparticles (denoted as 'algae-NP-robot') for the in vivo treatment of lung infection (Fig. 1a). *C. reinhardtii*-based microswimmers have been recently used as the microcarriers of synthetic cargo, demonstrating efficient movement and biocompatibility[15,16]. They can be facilely cultured and offer self-propulsion based on flagella beating (≥110 μm s^{-1}), intrinsic autofluorescence, phototactic guidance and a long lifespan[17]. Neutrophil membrane-coated NPs are used because of their unique cell-mimicking properties, including shielding payloads from biological environments, reducing immune clearance and enabling specific binding with target pathogens[18]. The unique properties of natural algae are combined with the engineering versatility of biomimetic NPs to yield a hybrid microrobot platform capable of active drug delivery.

Among the numerous applicable conditions, we choose to first test the algae-NP-robot for in vivo antibiotic delivery to treat bacterial lung infections. Specifically, ventilator-associated pneumonia (VAP) is an acute and potentially fatal infection characterized by onset 48 h after the initiation of mechanical ventilation in intensive care unit (ICU) settings[19]. VAP represents one of the most common infections among hospital patients, affecting between 10% and 25% of those who are intubated[20], resulting in considerable mortality, prolonged ICU stays and an increased number of days on ventilation[21–23]. Multidrug-resistant pathogens such as *Pseudomonas aeruginosa* are becoming increasingly prevalent as antibiotics continue to be indiscriminately used and with waning effectiveness[24]. We hypothesized that pulmonary antibiotic delivery efficiency could benefit from the deep tissue penetration and prolonged drug retention enabled by the algae-NP-robot system in an experimental model of VAP.

To transform microalgae into algae-NP-robot, we first modified the algal surface with azido *N*-hydroxysuccinimide (NHS)

[1]Department of NanoEngineering and Chemical Engineering Program, University of California San Diego, La Jolla, CA, USA. [2]Department of Pediatrics and Skaggs School of Pharmacy and Pharmaceutical Sciences, University of California San Diego, La Jolla, CA, USA. [3]These authors contributed equally: Fangyu Zhang, Jia Zhuang, Zhengxing Li, Hua Gong. ✉e-mail: zhang@ucsd.edu; josephwang@ucsd.edu

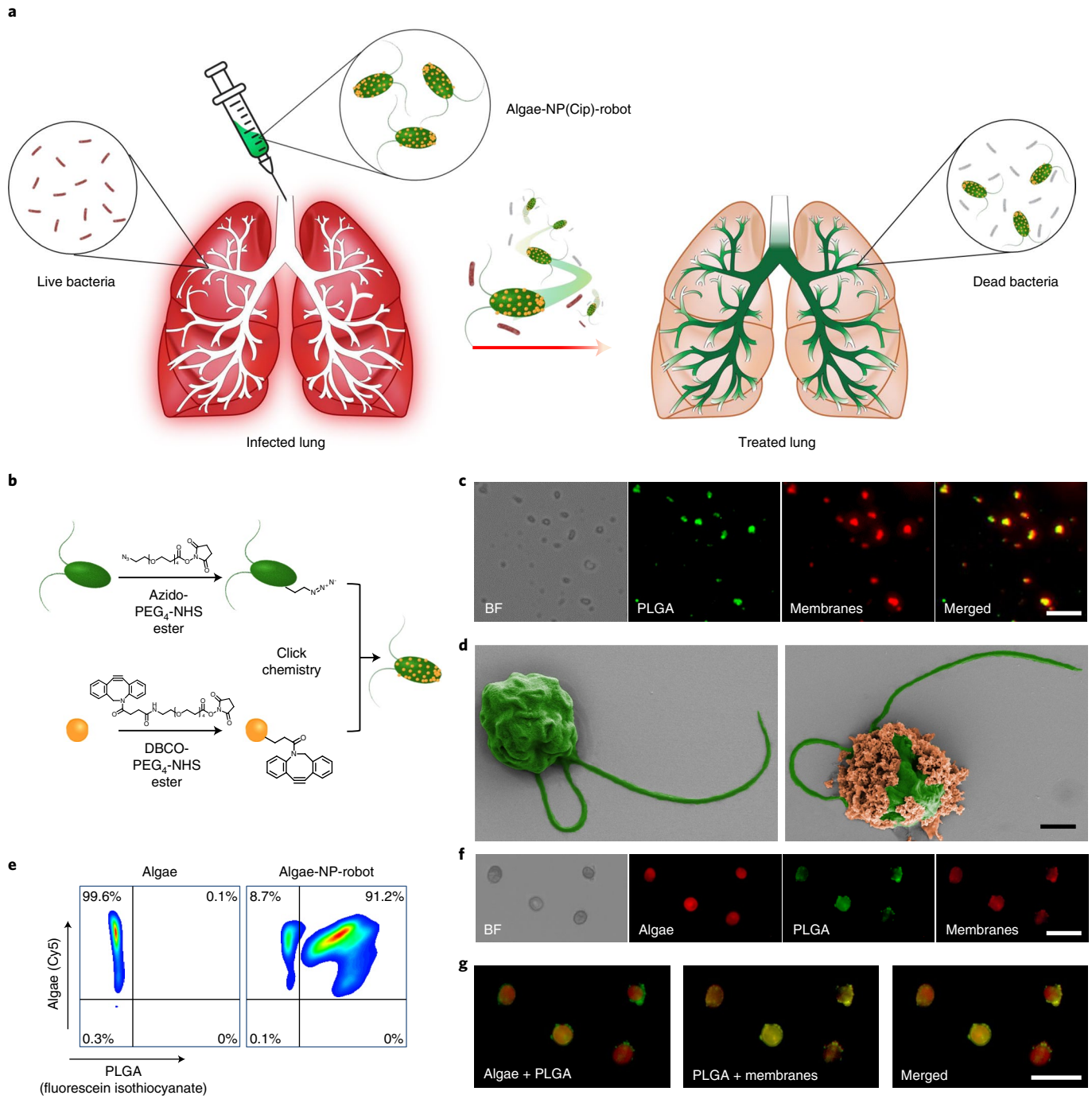

Fig. 1 | Preparation and structural characterization of the algae–nanoparticle hybrid microrobot (denoted as 'algae-NP-robot'). **a**, Schematic depicting the use of algae-NP-robot for the treatment of a bacterial lung infection. *C. reinhardtii* algae is modified with drug-loaded NPs and then administered in vivo for the treatment of *P. aeruginosa* lung infection. The NP consists of a neutrophil membrane-coated PLGA core. **b**, Schematic of the functionalization of *C. reinhardtii* with drug-loaded NP using click chemistry. **c**, Bright-field (BF) and fluorescent images of the NP, in which the PLGA cores are labelled with DiO (green colour) and the neutrophil membranes are labelled with DiI (red colour). Scale bar, 1 μm. **d**, Pseudo-coloured SEM images of an unmodified algae (left) and an algae-NP-robot (right). Scale bar, 2 μm. **e**, Flow cytometry analysis of algae before (left) and after (right) functionalization with DiO-labelled NPs. **f**, BF and fluorescent images of algae-NP-robot. Autofluorescence of natural algae chloroplast in the Cy5 channel; DiO-labelled PLGA cores in the GFP channel; DiI-labelled cell membranes in the RFP channel. Scale bar, 20 μm. **g**, Merged images from **f**. Cy5 and GFP channels (left); GFP and RFP channels (centre); all the three channels (right). Scale bar, 20 μm. In **c**, **f** and **g**, independent experiments were performed ($n = 3$) with similar results.

ester[25,26], followed by conjugation with dibenzocyclooctyne (DBCO)-modified neutrophil membrane-coated polymeric NPs via click chemistry (Fig. 1b). This type of reaction has been used to modify cells for a number of applications[27–29]. The motion and cargo-carrying behaviour of the resulting algae-NP-robot in simulated lung fluid (SLF), combined with their uniform distribution, effective inhibition of macrophage phagocytosis and prolonged retention in lung tissue, is verified and highlights the considerable

promise of the platform for in vivo drug delivery. Additionally, the therapeutic efficacy and safety of the drug-loaded algae-NP-robot are demonstrated using a murine model of *P. aeruginosa* lung infection.

Preparation of algae-NP-robot

C. *reinhardtii* algae were cultivated in a Tris-acetate-phosphate (TAP) medium (Supplementary Fig. 1). For further modification, the algae were conjugated with azido-PEG_4-NHS ester, which reacts with primary amines on the algal surface. The algae functionalization was confirmed, and negligible cytotoxicity was observed (Supplementary Fig. 2). We then fabricated neutrophil membrane-coated poly(lactic-*co*-glycolic acid) (PLGA) NPs[30] for use as a therapeutic payload. For visualization, the hydrophobic dyes 1,1′-dioctadecyl-3,3,3′,3′-tetramethylindocarbocyanine perchlorate (DiI) and 3,3′-dioctadecyloxacarbocyanine perchlorate (DiO) were loaded into the PLGA cores and neutrophil membranes, respectively. The overlap of both fluorescence signals indicated the successful association of the two components (Fig. 1c). The NPs were further characterized by dynamic light scattering, transmission electron microscopy (TEM) and immunostaining, verifying their core–shell structure and right-side-out membrane orientation (Supplementary Fig. 3). The surface of the NPs was further reacted with DBCO-PEG_4-NHS ester, and successful modification was qualitatively confirmed by fluorescence microscopy using an azide-functionalized dye (Supplementary Fig. 4). Conjugation to the algal surface was achieved through click chemistry by incubating the azido-modified algae with DBCO-modified NPs. Scanning electron microscopy (SEM) imaging confirmed the formation of NP-modified algae (Fig. 1d and Supplementary Fig. 5a,b). By optimizing the NP input concentration, 91.2% of the algae population could be conjugated with NPs (Fig. 1e and Supplementary Fig. 5c). Fluorescence microscopy was used to confirm that the NPs were firmly attached to the algal surface after multiple washing steps (Fig. 1f,g).

Motion behaviour of algae-NP-robot

The speed of algae-NP-robot ($104.6 \pm 11.2\,\mu m\,s^{-1}$) was similar to that of bare algae ($115.5 \pm 11.8\,\mu m\,s^{-1}$) in TAP medium at 22 °C (Supplementary Fig. 6a), suggesting that NP coupling had a negligible effect on algal motility. As we sought to leverage algae-NP-robot for deep lung delivery, propulsion characteristics in SLF[31] were first evaluated (Supplementary Table 1). The motion behaviour of bare algae at room temperature (RT, 22 °C) and at body temperature (BT, 37 °C) in SLF was compared (Fig. 2a–c and Supplementary Video 1). The bare algae maintained a steady speed of ~$115\,\mu m\,s^{-1}$ (11.5 body lengths per second) over 1 h at RT but displayed a gradual decrease in speed from ~101 to ~$55\,\mu m\,s^{-1}$ at BT, indicating that higher temperatures could impact algal motion[32]. The growth rate of bare algae was monitored at both temperatures, and an inhibition of growth was observed at BT[33] (Supplementary Fig. 6b). Algae-NP-robot demonstrated similar trends in their motion (Fig. 2d–f). To mimic the elevated BT of patients with VAP, an additional test was carried out at 40 °C, and no significant differences were observed compared with algae-NP-robot at BT. Figure 2g–l shows the representative tracking trajectories of individual algae-NP-robot over 0, 1 and 2 s intervals (Supplementary Video 2) and the corresponding mean speed distribution in SLF at different operation times at BT. It is important to note that 95% of the algae remained viable after 1 h of motion in SLF, reflecting the good adaptivity of algae under these conditions (Supplementary Fig. 6c,d). At longer timepoints of 12 and 24 h, approximately 85% and 60% of the algae-NP-robot, respectively, remained motile when exposed to SLF in the dark at BT; this percentage further decreased to less than 20% after 48 h of exposure (Supplementary Fig. 6e and Supplementary Video 4). Algae-NP-robot did not exert cytotoxicity when incubated with different cell types (Supplementary Fig. 7), and their capacity for phototaxis was unaffected (Supplementary Fig. 8 and Supplementary Video 5). Overall, these results demonstrate that modification with NPs has a negligible effect on the intrinsic motion behaviour of algae, allowing algae-NP-robot to be employed as an active delivery platform in physiological conditions.

In vivo distribution, retention and clearance in the lungs

The lung distribution of algae-NP-robot was examined after intratracheal administration[34]. Leveraging autofluorescence from the algae's chloroplasts, the distribution was visualized by ex vivo fluorescence imaging of the excised lungs at various timepoints (Fig. 3a). Fluorescence from the algae-NP-robot permeated throughout the lung tissue within 1 h, and the strong signal was retained for at least 24 h. In contrast, NP-modified deflagellated algae (denoted as 'static algae-NP'), incapable of moving, were characterized by SEM and used as a control (Supplementary Fig. 9). The signal of static algae-NP sharply decreased within 4 h and nearly disappeared after 12 h, highlighting the role of active motion in promoting robust lung distribution and retention. To quantitatively compare algal retention, we homogenized the lungs and measured the fluorescence intensity. The total fluorescence of the algae-NP-robot slowly decreased over the course of 72 h and was significantly higher than that of the static algae-NP up to 48 h. After 72 h, the fluorescence intensity returned to near the baseline for both groups (Supplementary Fig. 10). The normalized fluorescence data further verified the slower clearance of algae-NP-robot, as 86% and 65% of the original signal were present at 4 and 24 h, respectively (Fig. 3b). In comparison, static algae-NP exhibited greatly reduced signals, with 24% and 8% remaining at 4 and 12 h, respectively. Overall, these data indicate that the motion behaviour of algae-NP-robot greatly improved their lung retention.

To better understand the greatly reduced clearance of algae-NP-robot compared with static algae-NP, we sought to elucidate the potential role of macrophages, an abundant cell population in the lung alveoli capable of clearing exogenous species by phagocytosis[35]. Algae-NP-robot and static algae-NP were mixed with murine J774 macrophages at a 1:1 ratio and incubated at 37 °C in the dark. Figure 3c displays the different stages of the algae-NP-robot phagocytosis by macrophages. Algae-NP-robot showed strong autofluorescence from the algae before binding and on contacting the macrophage (0 min). After being taken up by the macrophages via phagocytosis, the algae-NP-robot was gradually degraded, as indicated by a progressive decrease in autofluorescence (15–75 min). By counting the numbers of unbound algae-NP-robot and macrophages at different timepoints (Supplementary Fig. 11a), the uptake of algae-NP-robot over time was quantified. As shown in Fig. 3d, static algae-NP were internalized significantly faster than their active counterparts, indicating that active motion facilitates escape from macrophage uptake (Supplementary Video 3). A cryo-treated algae-NP-robot, incapable of moving, was also taken up faster by macrophages compared with algae-NP-robot, confirming that the physical presence of flagella is not a major factor in the inhibition of phagocytosis (Supplementary Fig. 11b). Quantification of the total fluorescence intensity showed that the signal of the algae-NP-robot was consistently higher than that of the static control during 72 h of incubation (Supplementary Fig. 12a). Compared with the uptake profiles (Fig. 3d), the relative fluorescence profiles of the algae were reversed (Fig. 3e). It should be noted that the optical absorbance and fluorescence of the algae-NP-robot without the macrophages was constant (Supplementary Fig. 12b,c), further supporting that macrophage phagocytosis was an important reason for the observed lung-clearance kinetics.

To better understand the clearance mechanism in vivo, flow cytometry analysis of the macrophage uptake was performed at different timepoints after intratracheal administration in mice

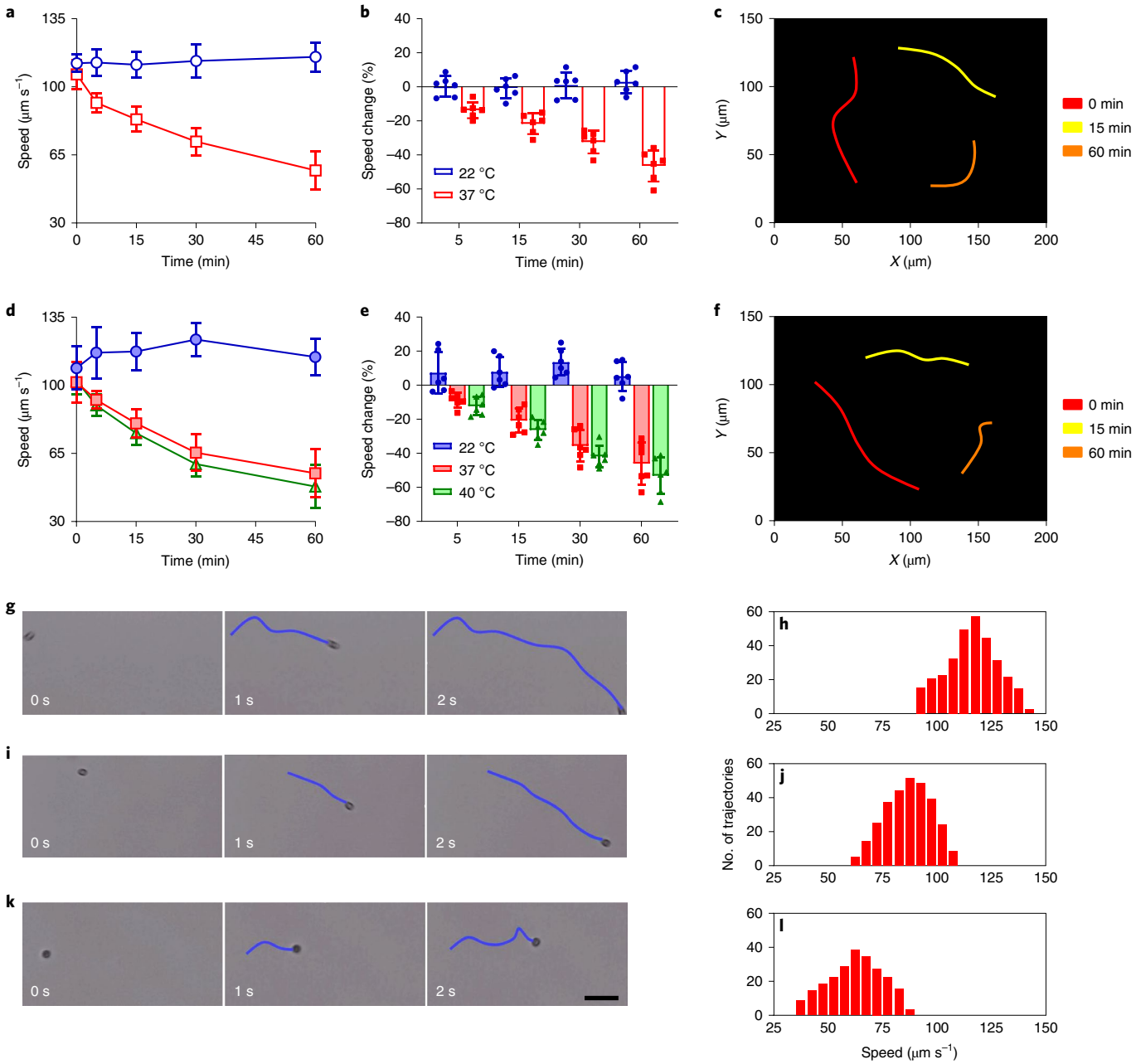

Fig. 2 | Motion behaviour of algae-NP-robot. a–f, Comparison of the speed of bare algae (**a** and **b**) and algae-NP-robot (**d** and **e**) in simulated lung fluid (SLF) at room temperature (22 °C), body temperature (37 °C) and elevated body temperature (40 °C) (blue, red and green bars, respectively) ($n = 6$; mean ± standard deviation (s.d.)). Optical tracking trajectories of the motion of bare algae (**c**) and algae-NP-robot (**f**) in SLF at 37 °C over 1 s (obtained at 0, 15 and 60 min: red, yellow and orange, respectively) (Supplementary Video 1). **g–l**, Representative trajectories (**g**, **i** and **k**) from Supplementary Video 2 corresponding to 0, 1 and 2 s, respectively, and mean speed distribution (**h**, **j** and **l**) of algae-NP-robot in SLF at 37 °C after 0 min (**g** and **h**), 15 min (**i** and **j**) and 60 min (**k** and **l**). Scale bar, 50 μm.

(Fig. 3f,g and Supplementary Fig. 13). A minimal uptake of algae-NP-robot by alveolar macrophages was observed within the first 12 h, and a large increase of uptake was observed at 48 h. In comparison, approximately 20% of the macrophages were positive for static algae-NP uptake after only 1 h, with the uptake peaking at 4 h post-administration before decreasing at later timepoints. The decreased signal is attributed to the degradation of algae after uptake, which destroys their autofluorescence (Fig. 3c). These results indicate that alveolar macrophage uptake is a major clearance mechanism for algae in the lungs. The delayed in vivo uptake of the algae-NP-robot by alveolar macrophages corroborates the in vitro findings and could explain the enhanced lung retention that was observed.

Drug loading and in vivo antibacterial efficacy

Based on the uniform lung distribution and prolonged retention, we postulated that algae-NP-robot may serve as an effective drug carrier for treating infection in the lower respiratory tract. In the study, ciprofloxacin (Cip), a common antibiotic drug used in combinational regimens against susceptible strains of *P. aeruginosa*, was encapsulated into NP (denoted as 'NP(Cip)'). The drug loading was optimized to meet the therapeutic threshold for *P. aeruginosa*[36].

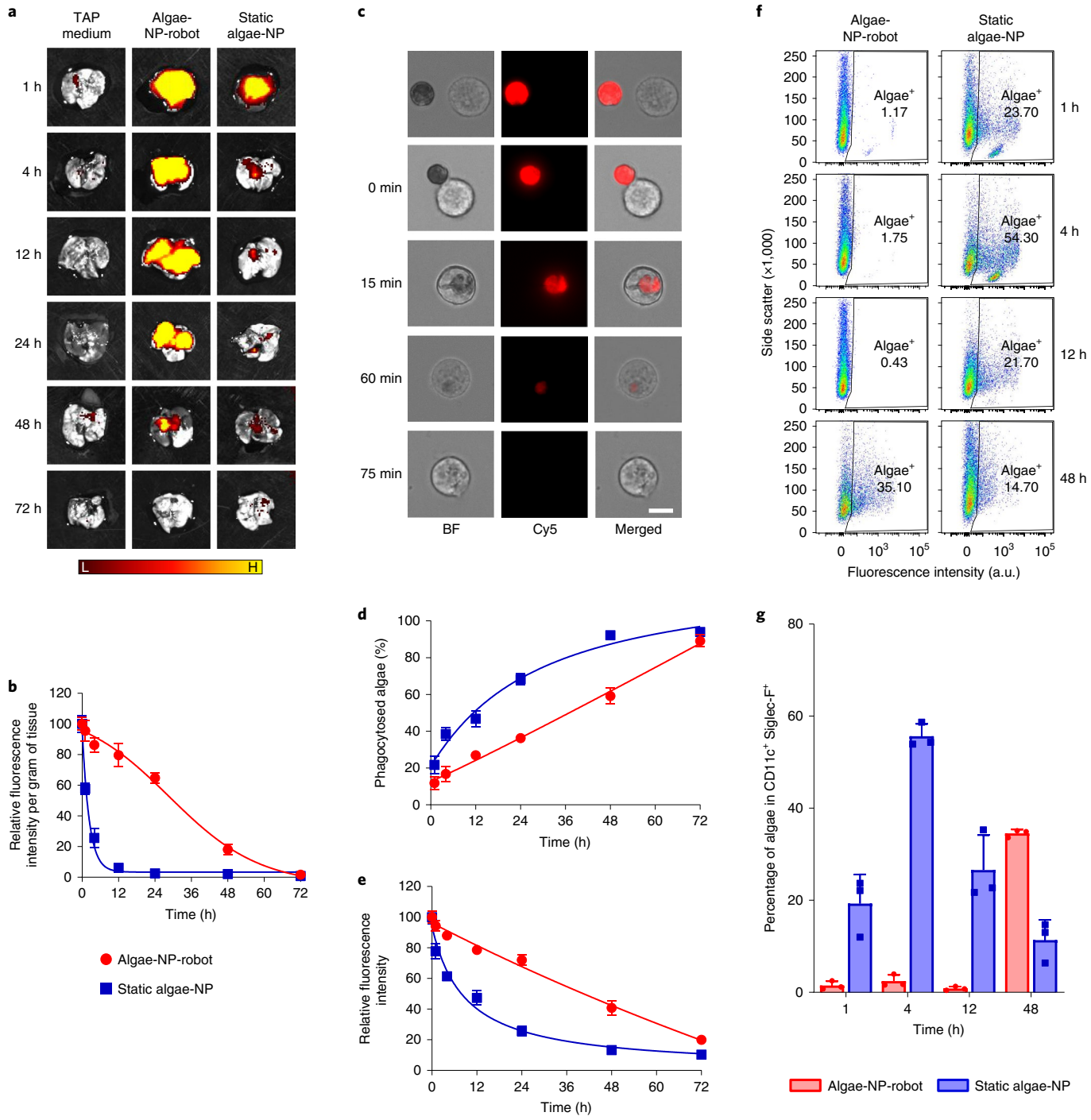

Fig. 3 | Lung distribution of algae-NP-robot. a, Ex vivo fluorescent imaging of lungs at various timepoints after intratracheal administration with TAP medium, algae-NP-robot or static algae-NP (negative control) (H, high signal; L, low signal). **b**, Normalized intensity per gram of tissue of lung samples collected in **a** ($n = 3$; mean + s.d.). **c**, BF and fluorescence microscopy images of representative algae-NP-robot incubated with macrophages at various stages of their interaction. Scale bar, 10 μm. Independent experiments ($n = 3$) were performed with similar results. **d**, Macrophage phagocytosis of static algae-NP or algae-NP-robot over time ($n = 3$; mean + s.d.). **e**, Relative fluorescence intensity of algae-NP-robot or static algae-NP over time after incubation with macrophage cells in vitro ($n = 3$; mean + s.d.). **f**, Representative flow cytometry dot plots of algae-NP-robot (left) and static algae-NP (right) uptake by alveolar macrophages ($CD11c^+$ $Siglec\text{-}F^+$) at various timepoints after intratracheal administration in vivo. **g**, Comparison of algae-NP-robot and static algae-NP uptake in alveolar macrophages at various timepoints after intratracheal administration in vivo ($n = 3$; mean + s.d.).

The same method as before was used to fabricate algae conjugated with the drug-loaded NPs (denoted as 'algae-NP(Cip)-robot'). We then evaluated the Cip loading yield onto the algae (Fig. 4a). Using a constant drug input, the total amount of Cip loaded increased linearly with algae number up to approximately 4×10^7 algae and then slowly saturated. The formulation consisting of 6 μg Cip loaded onto 4×10^7 algae was thus selected for subsequent in vitro and in vivo studies. Similar to NP(Cip), algae-NP(Cip)-robot demonstrated an initial burst release of drug over the initial 20 h, followed by a slow release up to 96% by 72 h (Fig. 4b). The minimal

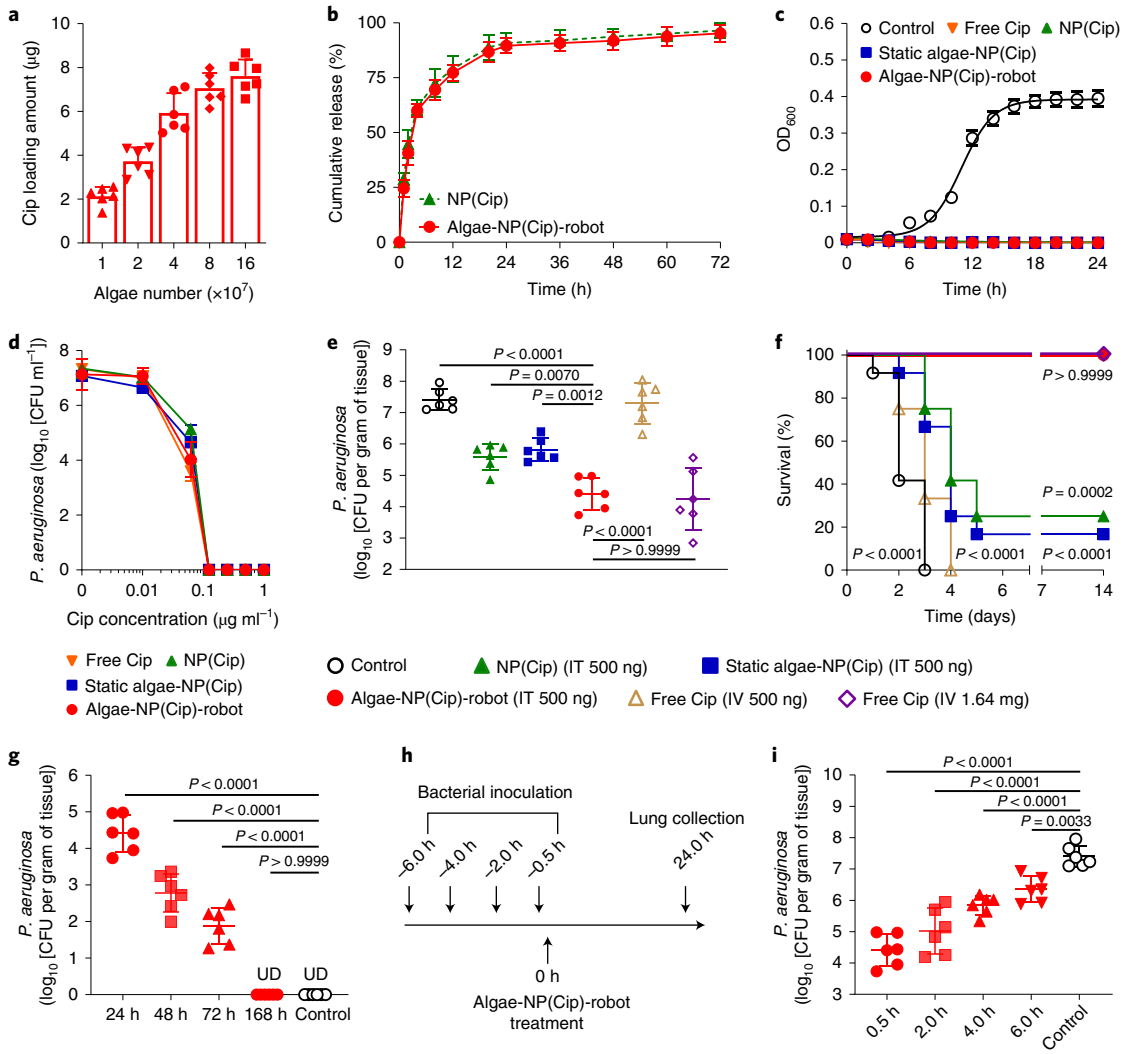

Fig. 4 | In vivo therapeutic efficacy of algae-NP-robot. a, Quantification of Cip loading on different numbers of algae ($n = 6$; mean + s.d.). **b**, Cumulative drug release profile of NP(Cip) and algae-NP(Cip)-robot ($n = 3$; mean + s.d.). **c**, Optical density at 600 nm (OD_{600}) measurements of *P. aeruginosa* treated with the control TAP medium, free Cip, NP(Cip), static algae-NP(Cip) and algae-NP(Cip)-robot ($n = 3$; mean + s.d.). **d**, In vitro antibacterial activity of free Cip, NP(Cip), static algae-NP(Cip) and algae-NP(Cip)-robot against *P. aeruginosa* ($n = 3$; geometric mean + s.d.). **e**,**f**, In vivo antibacterial efficacy of the control TAP medium, NP(Cip), static algae-NP(Cip) and algae-NP(Cip)-robot with a dosage of 500 ng by intratracheal (IT) administration and free Cip with the same dosage of 500 ng as used in intratracheal administration and a clinical dosage of 1.64 mg by IV administration in *P. aeruginosa*-infected mice, as determined by bacterial enumeration ($n = 6$; geometric mean + s.d.) (**e**) and survival ($n = 12$ per group) (**f**) studies. **g**, Quantification of bacterial load in the lungs at 24, 48, 72 and 168 h after the algae-NP(Cip)-robot treatment ($n = 6$; geometric mean + s.d.). UD, undetectable. **h**,**i**, Experimental timeline (**h**) and data (**i**) for the enumeration of bacterial load in the lungs of mice treated with algae-NP(Cip)-robot at different times after challenge with *P. aeruginosa* ($n = 6$; geometric mean + s.d.). One-way analysis of variance for **e**, **g** and **i** and log-rank (Mantel–Cox) test for **f**.

inhibitory concentration against *P. aeruginosa* was then evaluated (Supplementary Fig. 14). Bacterial growth was inhibited at a Cip concentration of 62.5 ng ml^{-1} for all the groups (Fig. 4c), consistent with what has been previously reported[37]. Figure 4d shows the enumerated bacterial colony-forming units (CFU) after treatment with algae-NP(Cip)-robot and with other controls, enabling us to establish the minimal bactericidal concentration. Algae-NP(Cip)-robot had a comparable inhibitory efficacy to free Cip, and the minimal bactericidal concentration of both was determined to be 125 ng ml^{-1}. Bare algae and NPs had negligible effects on the bacteria, supporting the fact that the inhibitory efficacy of algae-NP(Cip)-robot was solely due to the loaded Cip (Supplementary Fig. 15). An in vitro study was also performed to confirm that the algae-NP-robot is able to bind to *P. aeruginosa*. After 24 h of incubation, a signal from the Hoechst 33342-stained DNA of the bacteria co-localized with that of the DiI-labelled NPs, demonstrating effective binding between the two (Supplementary Fig. 16a). The binding efficiency was further quantified by the enumeration of unbound bacteria, revealing that 95% of the initial bacterial input was bound to algae-NP-robot (Supplementary Fig. 16b). Such binding is thought to be mediated by protein receptors present on the surface of the NPs[38]. To further verify the unique binding properties of the NPs, PLGA NP cores without membrane coating and liposomes were used, and neither control bound effectively to the bacteria (Supplementary Fig. 17).

Next, we examined the ability of algae-NP(Cip)-robot to treat acute lung infection in vivo. *P. aeruginosa* was first inoculated to characterize the bacterial dispersion within the lungs (Supplementary Fig. 18). The data demonstrated that the bacteria disseminated throughout the entirety of the lungs within 1 h after intratracheal inoculation, suggesting that algae-NP-robot could be used to

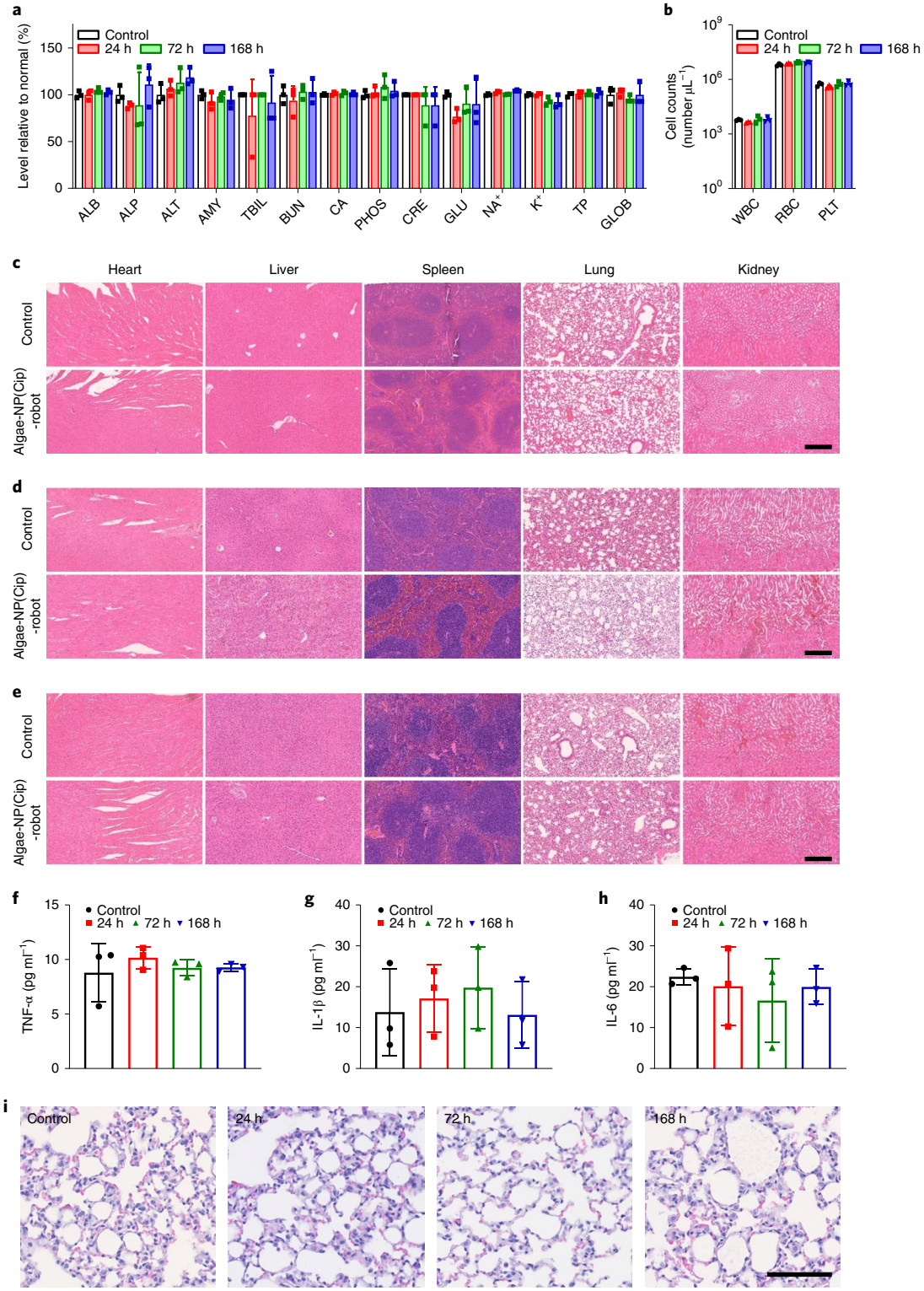

Fig. 5 | In vivo safety evaluation of algae-NP(Cip)-robot. a, Comprehensive blood chemistry panel taken 24 h after the intratracheal administration of TAP medium or 24, 72 and 168 h after that of algae-NP(Cip)-robot ($n = 3$; mean + s.d.). ALB, albumin; ALP, alkaline phosphatase; ALT, alanine transaminase; AMY, amylase; TBIL, total bilirubin; BUN, blood urea nitrogen; CA, calcium; PHOS, phosphorus; CRE, creatinine; GLU, glucose; NA^+, sodium; K^+, potassium; TP, total protein; GLOB, globulin. **b**, Counts of various blood cells 24 h after the intratracheal administration of TAP medium or 24, 72 and 168 h after that of algae-NP(Cip)-robot ($n = 3$; geometric mean + s.d.). WBC, white blood cells; RBC, red blood cells; PLT, platelets. **c**–**e**, Haematoxylin and eosin staining of histology sections from major organs 24 h (**c**), 72 h (**d**) and 168 h (**e**) after the intratracheal administration of TAP medium or algae-NP(Cip)-robot. Scale bars, 250 μm. Independent experiments ($n = 3$) were performed with similar results. **f**–**h**, Cytokines, including TNF-α (**f**), IL-1β (**g**) and IL-6 (**h**), measured in the BALF from healthy control mice or 24, 72 and 168 h after the intratracheal administration of algae-NP(Cip)-robot ($n = 3$; mean ± s.d.) **i**, Representative images of haematoxylin and eosin staining on lung histology sections taken from healthy control mice or 24, 72 and 168 h after the intratracheal administration of algae-NP(Cip)-robot. Scale bar, 100 μm. Independent experiments were performed ($n = 3$) with similar results.

efficiently treat conditions like VAP. To investigate the antibacterial efficacy against *P. aeruginosa* pneumonia, algae-NP(Cip)-robot or control samples were intratracheally administered 30 min after bacterial inoculation. An antibiotic dose of 500 ng Cip was administered per mouse (Supplementary Fig. 19). The lungs were then collected, followed by homogenization for bacterial enumeration 24 h after administration. As illustrated in Fig. 4e, the bacterial burden after the algae-NP(Cip)-robot treatment was quantified as 2.6×10^4 CFU g^{-1}, representing a three orders of magnitude reduction compared with the negative control (2.6×10^7 CFU g^{-1}), and a significant reduction compared with static algae-NP(Cip) (6.5×10^5 CFU g^{-1}) and NP(Cip) (3.8×10^5 CFU g^{-1}). A survival study was conducted using the same experimental setup (Fig. 4f). The algae-NP(Cip)-robot treatment of infected mice resulted in 100% survival over the entire duration of the 14-day study ($P<0.0001$, $n=12$). In stark contrast, all the untreated mice died within three days. The survival rates of mice treated with NP(Cip) or static algae-NP(Cip) were 25.0% and 16.7%, respectively. We concluded that the prolonged lung retention and sustained release characteristics of algae-NP(Cip)-robot enabled the significant improvement in survival compared with the control groups. Subsequently, we compared the efficacy of algae-NP(Cip)-robot with the conventional treatment of intravenous (IV) Cip. The algae-NP(Cip)-robot treatment significantly outperformed IV Cip at the same drug dosage (500 ng per mouse) and achieved similar efficacy compared with IV Cip at a more clinically relevant dosage (1.644 mg per mouse). Additional experiments were performed to quantify the lung bacterial burden at later timepoints following algae-NP(Cip)-robot treatment, revealing a progressive decrease over time and complete clearance after one week (Fig. 4g). To verify the effectiveness of algae-NP(Cip)-robot with delayed treatment, we performed an additional study in which mice were treated at progressively longer intervals after a lethal *P. aeruginosa* challenge (Fig. 4h,i). Although the therapeutic efficacy decreased as the treatment interval increased, a significant reduction was still observed even with a 6 h delay.

Biosafety evaluation

Last, to verify the biosafety of algae-NP(Cip)-robot, a comprehensive analysis of blood chemistry and major blood cell populations was conducted 24, 72 and 168 h after administration into the lungs (Fig. 5a,b). Compared with mice administered only with the TAP medium, little difference was observed for all the blood parameters. The heart, liver, spleen, lungs and kidneys were also processed by haematoxylin and eosin staining (Fig. 5c–e). The overall structural integrity of all the tissues was nearly identical to those from mice administered with the TAP medium, demonstrating no signs of acute toxicity and further supporting the safety of algae-NP(Cip)-robot. To further evaluate for potential inflammatory responses in the lungs, different cytokines (tumour necrosis factor alpha (TNF-α), interleukin (IL)-1β and IL-6) were analysed 24, 72 and 168 h after the intratracheal administration of algae-NP(Cip)-robot into the lungs. No significant difference in cytokine levels was observed for the algae-NP(Cip)-robot treatment compared with the control group (Fig. 5f–h). Histological sections of lung tissues collected over time at 24, 72 and 168 h after administration revealed negligible leucocyte infiltration, normal structures of the lung tissue and no signs of inflammation (Fig. 5i). Further in vitro studies verified that algae-NP-robot, in contrast to bacterial flagellin[39], did not trigger the significant production of proinflammatory cytokines by innate immune cells (Supplementary Fig. 20). Together, these data suggest the favourable safety profile of the algae-NP-robot delivery platform.

Outlook

The biohybrid microrobot platform described in this work creates new opportunities for active drug delivery to the lungs of ventilated ICU patients. This is due to its distinct advantages in terms of facile large-scale production, autonomous motion and long lifespan in localized environments, intrinsic autofluorescence for easy in vivo observation and potential targeting functionality. Further studies are required to determine if our biohybrid microrobot system can deliver key antibiotics for treating other important bacterial pathogens in VAP, including *Acinetobacter baumannii* and *Staphylococcus aureus*, or be extended to the treatment of other ICU conditions such as acute respiratory distress syndrome—a complication of viral pneumonia. Future studies will also test the algae-NP-robot formulation against clinical *P. aeruginosa* isolates to evaluate its general applicability. In its current iteration for intratracheal administration, the biohybrid microrobot would not be suitable for treating chronic *P. aeruginosa* infections, such as those that afflict the lungs of cystic fibrosis patients, or for other patients in which mechanical ventilation or bronchoscopy is not indicated by their clinical status. Before human clinical trials, additional validation using large animal models suitable for repeated dosing studies would enable a better evaluation of the algae-NP-robot therapeutic efficacy and safety in comparison to clinical IV antibiotic regimens. Looking forward, it would also be interesting to more precisely understand how algae-based microrobots interact with the immune system, aiming to further improve their retention time in the lungs. Exploring different delivery methods, such as by inhalation or IV administration, or leveraging the inherent phototaxis properties of algae, may expand the scope of the platform across a wider range of applications.

Although the treatment of acute pneumonia using algae-NP-robot probably benefited from uniform dispersion throughout the lungs, biohybrid microrobots can also be integrated with sensory and targeting functionalities for situations in which more precise delivery is required. For example, optogenetics technology that locally induces the light emission of target cells with photoreceptors[40] can be introduced to trigger the inherent phototaxis of algae[41], thus enabling site-specific targeting[42]. The algae can also be genetically engineered with functional proteins on their surface to introduce additional functionalities[43]. Besides algae, other microorganisms with specific sensory or targeting capabilities[13,44] could also be used in the development of autonomous drug delivery vehicles for treating pulmonary diseases.

Online content

Any methods, additional references, Nature Research reporting summaries, source data, extended data, supplementary information, acknowledgements, peer review information; details of author contributions and competing interests; and statements of data and code availability are available at https://doi.org/10.1038/s41563-022-01360-9.

Received: 19 August 2020; Accepted: 9 August 2022;
Published online: 22 September 2022

References

1. Li, J. et al. Micro/nanorobots for biomedicine: delivery, surgery, sensing, and detoxification. *Sci. Robot.* **2**, eaam6431 (2017).
2. Gao, C. et al. Biomedical micro-/nanomotors: from overcoming biological barriers to in vivo imaging. *Adv. Mater.* **33**, 2000512 (2020).
3. Wu, Z., Chen, Y., Mukasa, D., Pak, O. S. & Gao, W. Medical micro/nanorobots in complex media. *Chem. Soc. Rev.* **49**, 8088–8112 (2020).
4. Esteban-Fernández de Ávila, B. et al. Micromotor-enabled active drug delivery for in vivo treatment of stomach infection. *Nat. Commun.* **8**, 272 (2017).
5. Wu, Z. et al. A microrobotic system guided by photoacoustic computed tomography for targeted navigation in intestines in vivo. *Sci. Robot.* **4**, eaax0613 (2019).
6. Wu, Z. et al. A swarm of slippery micropropellers penetrates the vitreous body of the eye. *Sci. Adv.* **4**, eaat4388 (2018).
7. Gao, W. et al. Artificial micromotors in the mouse's stomach: a step toward in vivo use of synthetic motors. *ACS Nano* **9**, 117–123 (2015).

8. Wei, X. et al. Biomimetic micromotor enables active delivery of antigens for oral vaccination. *Nano Lett.* **19**, 1914–1921 (2019).
9. Servant, A., Qiu, F., Mazza, M., Kostarelos, K. & Nelson, B. J. Controlled in vivo swimming of a swarm of bacteria-like microrobotic flagella. *Adv. Mater.* **27**, 2981 (2015).
10. Yan, X. et al. Multifunctional biohybrid magnetite microrobots for imaging-guided therapy. *Sci. Robot.* **2**, eaaq1155 (2017).
11. Sun, L. et al. Biohybrid robotics with living cell actuation. *Chem. Soc. Rev.* **49**, 4043–4069 (2020).
12. Ricotti, L. et al. Biohybrid actuators for robotics: a review of devices actuated by living cells. *Sci. Robot.* **2**, eaaq0459 (2017).
13. Felfoul, O. et al. Magneto-aerotactic bacteria deliver drug-containing nanoliposomes to tumour hypoxic regions. *Nat. Nanotechnol.* **11**, 941–947 (2016).
14. Medina-Sánchez, M., Schwarz, L., Meyer, A. K., Hebenstreit, F. & Schmidt, O. G. Cellular cargo delivery: toward assisted fertilization by sperm carrying micromotors. *Nano Lett.* **16**, 555–561 (2015).
15. Weibel, D. B. et al. Microoxen: microorganisms to move microscale loads. *Proc. Natl Acad. Sci. USA* **102**, 11963–11967 (2005).
16. Yasa, O., Erkoc, P., Alapan, Y. & Sitti, M. Microalga-powered microswimmers toward active cargo delivery. *Adv. Mater.* **30**, 1804130 (2018).
17. Silflow, C. D. & Lefebvre, P. A. Assembly and motility of eukaryotic cilia and flagella. Lessons from *Chlamydomonas reinhardtii*. *Plant Physiol.* **127**, 1500–1507 (2001).
18. Zhang, Q. et al. Neutrophil membrane-coated nanoparticles inhibit synovial inflammation and alleviate joint damage in inflammatory arthritis. *Nat. Nanotechnol.* **13**, 1182–1190 (2018).
19. Metersky, M. L. & Kalil, A. C. Management of ventilator-associated pneumonia: guidelines. *Clin. Chest Med.* **39**, 797–808 (2018).
20. Schreiber, M. P. & Shorr, A. F. Challenges and opportunities in the treatment of ventilator-associated pneumonia. *Expert Rev. Anti Infec. Ther.* **15**, 23–32 (2017).
21. Muscedere, J. et al. The clinical impact and preventability of ventilator-associated conditions in critically ill patients who are mechanically ventilated. *Chest* **144**, 1453–1460 (2013).
22. Melsen, W. G. et al. Attributable mortality of ventilator-associated pneumonia: a meta-analysis of individual patient data from randomised prevention studies. *Lancet Infect. Dis.* **13**, 665–671 (2013).
23. Kharel, S., Bist, A. & Mishra, S. K. Ventilator-associated pneumonia among ICU patients in WHO Southeast Asian region: a systematic review. *PLoS ONE* **16**, e0247832 (2021).
24. Vincent, J.-L., de Souza Barros, D. & Cianferoni, S. Diagnosis, management and prevention of ventilator-associated pneumonia. *Drugs* **70**, 1927–1944 (2010).
25. Kerschgens, I. P. & Gademann, K. Antibiotic algae by chemical surface engineering. *ChemBioChem* **19**, 439–443 (2018).
26. Szponarski, M. et al. On-cell catalysis by surface engineering of live cells with an artificial metalloenzyme. *Commun. Chem.* **1**, 84 (2018).
27. Shi, P. et al. Spatiotemporal control of cell–cell reversible interactions using molecular engineering. *Nat. Commun.* **7**, 13088 (2016).
28. Wang, H. et al. Metabolic labeling and targeted modulation of dendritic cells. *Nat. Mater.* **19**, 1244–1252 (2020).
29. Hu, Q. et al. Conjugation of haematopoietic stem cells and platelets decorated with anti-PD-1 antibodies augments anti-leukaemia efficacy. *Nat. Biomed. Eng.* **2**, 831–840 (2018).
30. Fang, R. H. et al. Cell membrane coating nanotechnology. *Adv. Mater.* **30**, 1706759 (2018).
31. Kumar, A. et al. A biocompatible synthetic lung fluid based on human respiratory tract lining fluid composition. *Pharm. Res.* **34**, 2454–2465 (2017).
32. Tanaka, Y. et al. Acclimation of the photosynthetic machinery to high temperature in *Chlamydomonas reinhardtii* requires synthesis de novo of proteins encoded by the nuclear and chloroplast genomes. *Plant Physiol.* **124**, 441–449 (2000).
33. Singh, S. P. & Singh, P. Effect of temperature and light on the growth of algae species: a review. *Renew. Sust. Energ. Rev.* **50**, 431–444 (2015).
34. Ortiz-Munoz, G. & Looney, M. R. Non-invasive intratracheal instillation in mice. *Bio-protocol* **5**, e1504 (2015).
35. Sibille, Y. & Reynolds, H. Y. Macrophages and polymorphonuclear neutrophils in lung defense and injury. *Am. Rev. Respir. Dis.* **141**, 471–501 (1990).
36. Justo, J. A., Danziger, L. H. & Gotfried, M. H. Efficacy of inhaled ciprofloxacin in the management of non-cystic fibrosis bronchiectasis. *Ther. Adv. Respir. Dis.* **7**, 272–287 (2013).
37. Oliver, A. et al. Hypermutation and the preexistence of antibiotic-resistant *Pseudomonas aeruginosa* mutants: implications for susceptibility testing and treatment of chronic infections. *Antimicrob. Agents Chemother.* **48**, 4226–4233 (2004).
38. Lovewell, R. R., Patankar, Y. R. & Berwin, B. Mechanisms of phagocytosis and host clearance of *Pseudomonas aeruginosa*. *Am. J. Physiol. Lung Cell. Mol. Physiol.* **306**, L591–L603 (2014).
39. Hayashi, F. et al. The innate immune response to bacterial flagellin is mediated by Toll-like receptor 5. *Nature* **410**, 1099–1103 (2001).
40. Boyden, E. et al. Millisecond-timescale, genetically targeted optical control of neural activity. *Nat. Neurosci.* **8**, 1263–1268 (2005).
41. Sineshchekov, O. A., Jung, K.-H. & Spudich, J. L. Two rhodopsins mediate phototaxis to low- and high-intensity light in *Chlamydomonas reinhardtii*. *Proc. Natl Acad. Sci. USA* **99**, 8689–8694 (2002).
42. Akolpoglu, M. B. et al. High-yield production of biohybrid microalgae for on-demand cargo delivery. *Adv. Sci.* **7**, 2001256 (2020).
43. Delalat, B. et al. Targeted drug delivery using genetically engineered diatom biosilica. *Nat. Commun.* **6**, 8791 (2015).
44. Martel, S. et al. Flagellated magnetotactic bacteria as controlled MRI-trackable propulsion and steering systems for medical nanorobots operating in the human microvasculature. *Int. J. Robot. Res.* **28**, 571–582 (2009).

Methods

Algae culture. Green *C. reinhardtii* algae (strain CC-125 wild-type mt+) were obtained from the Chlamydomonas Resource Center. The algae were transferred from the agar plate to TAP medium (Thermo Fisher Scientific) and cultivated at RT under cycles of 12 h sunlight and 12 h dark.

Neutrophil cell culture. Human neutrophil-like cells (HL-60, American Type Culture Collection, ATCC CCL-240) were cultured in RPMI 1640 (11875135, Gibco) with 1 v/v% penicillin–streptomycin (15140122, Gibco) and 10 v/v% foetal bovine serum (SH30541.03, Hyclone) in an incubator under 5% CO_2 at a temperature of 37 °C. The cells were regularly tested for mycoplasma.

Neutrophil cell membrane derivation. HL-60 plasma membrane was collected according to an established procedure[23]. Frozen cells were thawed and washed three times with 1× phosphate-buffered saline (PBS). The cells were lysed in a buffer consisting of 30 mM Tris-HCl, 75 mM sucrose, 225 mM D-mannitol, 0.2 mM ethylene glycol-bis(β-aminoethyl ether)-*N*,*N*,*N*′,*N*′-tetraacetic acid and phosphatase/protease inhibitor mixtures (Sigma-Aldrich). Next, the cells were homogenized using a Kinematica POLYTRON PT-10/35 probe homogenizer, and the cell membrane was collected through gradient centrifugation. A BCA kit (Pierce) was used to quantify the cell membrane content. The final cell membrane was stored in 0.2 mM EDTA at −80 °C for subsequent studies.

Synthesis of polymeric cores. Drug-loaded polymeric cores were synthesized following a reported method with slight modifications[45]. Briefly, 50 µl of 25 mg ml^{-1} Cip (HCl salt, Sigma-Aldrich) solution was emulsified in 500 µl chloroform solution containing 50 mg ml^{-1} 50:50 PLGA (0.67 dl g^{-1}, Lactel Absorbable Polymers) using an ultrasonic probe sonicator (Fisher Scientific) operating at a power of 10 W. The sonication lasted for 2 min with alternating cycles of 2 s power on and 2 s power off inside an ice bath. Then, the emulsion was transferred to 10 ml aqueous solution and sonicated for another 2 min. The emulsion was stirred for 4 h to completely evaporate the chloroform. All the samples were centrifuged for 5 min at 16,100×*g* and washed twice with ultrapure water, and lyophilized for future use. NPs loaded with DiO (excitation wavelength (λ_{ex})/emission wavelength (λ_{em}) = 484/501 nm; Thermo Fisher Scientific) were synthesized by replacing Cip with 1 mg ml^{-1} of the dye and then following the same method.

Synthesis of neutrophil membrane-coated NPs. Neutrophil membrane-coated NPs were synthesized by an established procedure[18]. Briefly, the neutrophil membranes were added into a solution containing PLGA cores at a polymer/membrane protein weight ratio of 1:1. The neutrophil membranes were coated onto the PLGA cores through 3 min of sonication in a bath sonicator (Fisher Scientific FS30D). The resulting membrane-coated NPs were separated from the solution by 5 min centrifugation at 16,100×*g* and washed twice with ultrapure water.

Characterization of neutrophil membrane-coated NPs. The size and surface charge of the neutrophil membrane-coated NPs were measured using dynamic light scattering (ZEN 3600 Zetasizer, Malvern). In addition, the morphology of the NPs was verified using transmission electron spectroscopy (FEI 200 kV Sphera). Bright-field (BF) and fluorescent images of neutrophil membranes labelled with DiI ($\lambda_{ex}/\lambda_{em}$ = 551/566 nm; Thermo Fisher Scientific) and DiO-loaded PLGA cores were taken on a fluorescence microscope (EVOS FL). To verify the orientation of the neutrophil membrane after coating, neutrophils (~2.5 × 10^6 cells) and neutrophil membrane-coated NPs (100 µl, 0.5 mg ml^{-1} protein content) were blocked in 1% bovine serum albumin (BSA, MilliporeSigma) for 30 min and then incubated with 1 µl of 100 mg ml^{-1} Alexa Fluor 488 anti-human CD11a (LFA-1) antibody (BioLegend) for 30 min. The total fluorescent intensity of the mixture was measured by a BioTek Synergy Mx microplate reader. To separate the unbound antibodies, the neutrophil samples were spun down at 3,000×*g* for 5 min, whereas neutrophil membrane-coated NPs were centrifuged for 5 min in 300-kDa-molecular-weight-cutoff Nanosep tubes at 5,000×*g*. The fluorescence intensity of the unbound antibodies was measured to determine the amounts bound to the neutrophils and NPs.

Preparation of algae-NP-robot. Green algae were washed with ultrapure water three times to remove any residual TAP medium, and they were subsequently resuspended in ultrapure water. Then, 1 × 10^7 algae were treated with 20 µM azido-PEG$_4$-NHS ester (Click Chemistry Tools) for 45 min at RT. To examine the effective binding of azido groups on the algae surface, the resulting algae were incubated with borondipyrromethene FL DBCO (Lumiprobe) for 30 min and then subjected to flow cytometry analysis (1 × 10^4 events were collected for analysis). Then, neutrophil membrane-coated PLGA NPs were modified with N_3 bonds for the click chemistry. Here the NPs were incubated with 40 µM DBCO-PEG$_4$-NHS ester for 1 h at RT. The presence of triple bonds on the NP surface was confirmed by adding FAM azide, 5-isomer (Lumiprobe) and visualized by fluorescence microscopy. Both the resulting algae and NPs were washed five times with ultrapure water, removing the unreacted NHS ester for the following conjugation. To optimize the binding efficiency, we used different concentrations of NPs, specifically 0.04, 0.20 and 1.00 mg ml^{-1}, for conjugation. During the conjugation, DBCO-modified NPs were incubated with azido-functionalized algae for 45 min. After 3 min centrifugation at 300×*g* and three washes with TAP medium, the resulting algae-NP-robot were collected for further characterization. Static algae-NP were prepared by removing the flagella from the algae using 0.5 M acetic acid, followed by the same procedure for NP conjugation. Cryo-treated algae-NP-robots were prepared by a cryogenic treatment in which the algae-NP-robot was immersed into liquid nitrogen for 45 s to maintain the structure of the algae.

Characterization of algae-NP-robot. To perform SEM characterization, algae-NP-robots were first fixed with 2.5% glutaraldehyde overnight at 4 °C and then washed in ultrapure water. After overnight drying, algae-NP-robots were coated with palladium for SEM characterization using an acceleration voltage of 3 kV (Zeiss Sigma 500 SEM instrument). Bare algae and static algae-NP were treated and examined using the same methodology. The attachment of NPs to the algae was captured by fluorescence microscopy (EVOS FL) with three individual fluorescence channels, namely cyanine 5 (Cy5), red fluorescent probe (RFP) and green fluorescent probe (GFP), which corresponded to the autofluorescence of algae, DiI-labelled neutrophil membranes and DiO-loaded PLGA cores, respectively.

Algae viability study. To evaluate algae viability, algae were stained in 5 µM SYTOX GFP (Thermo Fisher). The bright green fluorescence of dead algae was examined by fluorescence microscopy. Based on previously reported methods[46], the solution was measured for SYTOX fluorescence intensity ($\lambda_{ex}/\lambda_{em}$ = 504/523 nm) using a plate reader. No washing steps were required due to the specific staining of the nucleic acid of dead algae.

Motion analysis. The motion of algae-NP-robot and bare algae control was evaluated in SLF. The SLF composition is shown in Supplementary Table 1. The speed of algae-NP-robot in SLF was measured in the dark at 37 °C, and changes in the motion were evaluated at 1, 12, 24 and 48 h. The speed of algae-NP-robot was also measured over 1 h at an elevated BT of 40 °C. The videos of the motion were recorded by an optical microscope (Nikon ECLIPSE Ti-S/L100). An NIS-Elements tracking module was used to measure the corresponding algae speed in SLF.

Binding of NPs or liposomes with bacteria. Neutrophil membrane-coated DiO-loaded PLGA NPs and DiO-loaded PLGA NP cores without membrane coating were prepared as before. Liposomes were synthesized through an extrusion-based method. Briefly, L-α-phosphatidylcholine (EggPC, Avanti Polar Lipids 840051) and cholesterol (Avanti Polar Lipids 700100) were dissolved in chloroform and mixed in a weight ratio of 9:1. To label the liposomes, DiO was dissolved in chloroform and added to the lipid mixture to reach a weight percentage of 2% DiO. The chloroform was evaporated in nitrogen gas. The dried lipid film was hydrated with sterile PBS to reach a total lipid concentration of 5 mg ml^{-1}. The lipid solution was vortexed for 1 min, followed by sonication in a bath sonicator. The rehydrated lipids were further extruded through a polycarbonate membrane with 100 nm pore size to form the liposomes. To compare the binding effect, 1 mg NPs, 1 mg PLGA NP cores without membrane coating and 1 mg liposomes were incubated with 1 × 10^7 ml^{-1} *P. aeruginosa* overnight. The unbound NPs, liposomes and PLGA NP cores without membrane coating were removed through three washing steps by centrifuging at 700×*g* for 2 min. BF and fluorescent images of the three groups were taken on a Life Technologies EVOS FL fluorescence microscope. The fluorescence values from DiO ($\lambda_{ex}/\lambda_{em}$ = 484/501 nm) were quantified using a BioTek Synergy Mx microplate reader. To perform SEM characterization, the samples were initially fixed overnight with 2.5% glutaraldehyde at 4 °C, followed by washing with ultrapure water. After overnight drying, the samples were coated with palladium for SEM characterization using an acceleration voltage of 3 kV (Zeiss Sigma 500 SEM instrument).

Binding of algae-NP-robot with bacteria. The PLGA core and neutrophil membrane were labelled with DiO and DiI, respectively. The algae-NP-robot was prepared as before. *P. aeruginosa* was labelled with Hoechst 33342 (Thermo Fisher Scientific) for 30 min at RT. The free dye was removed through three washing steps by centrifuging at 3,000×*g* for 5 min. To explore the binding effect between algae-NP-robot and bacteria, 1 × 10^5 ml^{-1} algae-NP-robot were incubated with 1 × 10^7 ml^{-1} *P. aeruginosa* overnight. The unbound bacteria were removed through five washing steps by centrifuging at 200×*g* for 2 min. After fixation in 2.5% glutaraldehyde, BF and fluorescent images of the binding between algae-NP-robot and *P. aeruginosa* were taken on a Life Technologies EVOS FL fluorescence microscope. To quantify the binding efficiency, 5 × 10^6 ml^{-1} algae-NP-robots were incubated with 5 × 10^6 CFU ml^{-1} *P. aeruginosa* for 1 h. Colonies of total bacterial input and unbound bacteria were counted after 24 h of culture on agar plates.

Cytotoxicity test. To evaluate the cytotoxicity, J774A.1 cells (ATCC TIB-67) and NL20 cells (ATCC CRL-2503) were seeded in 96-well plates at 1 × 10^4 cells per well. The cells were then incubated with algae-NP-robot with an algae/cell ratio of

0.0625, 0.1250, 0.2500, 0.5000, 1.0000, 2.0000, 4.0000, 8.0000, 16.0000, 32.0000 and 64.0000 for 24 h. CellTiter AQueous One Solution cell proliferation assay (Promega) was used to evaluate cell viability according to the manufacturer's instructions.

Phototaxis of algae-NP-robot. A small 2 µl droplet of algae-NP-robot was placed on a glass slide without further modification. After 5 s of random motion, the algae-NP-robot sample was illuminated with white light from the top for 30 s. The video was recorded using an optical microscope.

Intratracheal administration. Intratracheal administration was performed using a modified method based on a previous paper[34]. Specifically, male CD-1 mice (Charles River Labs) were placed under anaesthesia with a ketamine (Pfizer) and xylazine (Lloyd Laboratories) cocktail administered at 100 and 20 mg kg^{-1}, respectively. To prepare the inoculation, a certain volume of test materials (50 µl algae-NP-robot, static algae-NP, NPs and TAP medium) was injected into the polytetrafluoroethylene feeding tube (cut six to eight inches in length) by an insulin needle. Then, the feeding tube was inserted 0.5–1.0 cm into the trachea and the inoculum of test materials was administered into the lungs. To avoid escape of the test materials from the lungs, the feeding tube was left in place for 30 s.

Ex vivo lung imaging and retention quantification. All the animal experiments were approved by the Institutional Animal Care and Use Committee of the University of California San Diego and performed under the National Institutes of Health guidelines. Male CD-1 mice (Charles River Labs) were placed under anaesthesia with a ketamine and xylazine cocktail. They were subsequently intratracheally administrated with the TAP medium, 5×10^6 algae-NP-robot or 5×10^6 static algae-NP. After certain timepoints (1, 4, 12, 24, 48 and 72 h), the mice were euthanized, and their lungs were excised for analysis. Fluorescent ex vivo lung images were obtained with a Xenogen IVIS 200 system. Subsequently, the lung samples were homogenized, and the fluorescence values were measured on a BioTek Synergy Mx microplate reader. Bacterial dispersion studies were performed with a similar method. Briefly, *P. aeruginosa* bacteria were labelled with 1,1'-dioctadecyl-3,3,3',3'-tetramethylindodicarbocyanine, 4-chlorobenzenesulfonate salt (DiD; $\lambda_{ex}/\lambda_{em}$ 644/665 nm; Thermo Fisher Scientific) after overnight incubation. Following anaesthesia, the mice were intratracheally inoculated with 5×10^6 CFU of DiD-labelled *P. aeruginosa*. After 1 h inoculation, the mice were euthanized, and their lungs were excised for IVIS imaging analysis.

In vitro macrophage phagocytosis. J774A.1 macrophage cells were cultured using Dulbecco's modified Eagle medium (Invitrogen) in a 24-well plate at a density of 1×10^6 cells per well. Algae-NP-robots were then added at a robot/macrophage ratio of 1:1 and incubated at 37 °C. After certain timepoints (1, 4, 12, 24, 48 and 72 h), the mixture was analysed by fluorescence microscopy, and the fluorescence values were quantified using a BioTek Synergy Mx microplate reader. Static algae-NP and cryo-treated algae-NP-robot controls were tested and quantified following the same method.

Algae-NP-robot clearance in vivo. At various timepoints (1, 4, 12 and 48 h) before the study, male CD-1 mice were intratracheally inoculated with equivalent amounts of algae-NP-robot or static algae-NP. Then, the mice were euthanized by CO_2 asphyxiation and the trachea was exposed. A catheter made by tightly fitting a 23-gauge needle into polytetrafluoroethylene tubing (Cole Parmer) was inserted into the trachea and secured with sutures. Bronchoalveolar lavage fluid (BALF) was then collected from each mouse by repeatedly washing the lungs five times with 1 ml of 0.5% (v/v) foetal bovine serum (Gibco) and 2 mM EDTA in PBS and immediately stored on ice. The cells were spun down at 700×*g* for 5 min, and red blood cells were lysed using a commercial buffer (BioLegend) following the manufacturer's instructions. Subsequently, non-specific binding on the cells was blocked with 1% (w/v) BSA in PBS for 15 min and then probed with Pacific Blue-conjugated anti-mouse CD11c (N418, BioLegend) and PE-conjugated anti-mouse Siglec-F (S17007L, BioLegend) for 30 min on ice. The unbound antibodies were washed out twice with 1% BSA in PBS, and the cells were resuspended in 1% BSA in PBS for flow cytometry analysis. The data were acquired with a BD FACSCanto II flow cytometer and analysed using the FlowJo v.10 software.

Cip loading and release measurement. A total of 1 ml algae at different concentrations (1, 2, 4, 8 and 16×10^7 ml^{-1}) was conjugated with 1 mg NP(Cip) by click chemistry, followed by the removal of free NP(Cip) by three washes at 300×*g* for 2 min. Then, the algae-NP(Cip)-robots were suspended in 1 ml TAP for further use. After the fabrication of algae-NP(Cip)-robot, the solution was measured for Cip fluorescence intensity ($\lambda_{ex}/\lambda_{em}$ = 270/440 nm). A standard calibration curve was made by measuring the serial dilutions of Cip solution (0–10 µg ml^{-1}), and the Cip concentration was determined by comparing with the standard calibration curve. The Cip release study was conducted with 1 ml algae-NP(Cip)-robot at 37 °C over 72 h. The Cip concentration was determined by fluorescence measurement.

In vitro antibacterial activity of algae-NP(Cip)-robot. A volume of 1 ml *P. aeruginosa* PAO1 strain (ATCC, BAA-47) at 5×10^6 CFU ml^{-1} was mixed with TAP, free Cip, NP(Cip), static algae-NP(Cip) or algae-NP(Cip)-robot at an equivalent Cip amount. To quantify the minimal inhibitory concentration of Cip, various concentrations of Cip were used: 31.25 ng ml^{-1}, 62.50 ng ml^{-1}, 125.00 ng ml^{-1}, 250.00 ng ml^{-1}, 500.00 ng ml^{-1} and 1.00 µg ml^{-1}. The bacterial growth was quantified by measuring their absorbance at 600 nm (OD_{600}).

In vivo enumeration study. *P. aeruginosa* was first streaked onto a Luria broth (Sigma-Aldrich) agar plate and cultured overnight at 37 °C. A single colony was inoculated in 50 ml Luria broth and further cultured for 10 h at 37 °C on a shaker. The bacteria were collected after spinning down at 5,000×*g* for 20 min, washing with PBS and resuspending in PBS to a final concentration of 2×10^8 CFU ml^{-1}. Male CD-1 mice were placed under anaesthesia with a ketamine and xylazine cocktail. They were intratracheally inoculated with 5×10^6 CFU of *P. aeruginosa* and subsequently intratracheally administered with TAP medium, NP(Cip), 5×10^6 algae-NP(Cip)-robot or 5×10^6 static algae-NP(Cip) at an equivalent Cip amount (500 ng). After 24, 48, 72 and 168 h, the mice were euthanized, and their lungs were collected for the quantification of bacterial load. In a separate enumeration study, treatment with the algae-NP(Cip)-robot was delayed for 0.5, 2.0, 4.0 and 6.0 h after the bacterial challenge, and the lung samples were collected after another 24.0 h for enumeration. To compare with the IV treatment, an equivalent Cip amount (500 ng) and a clinical dose (1.64 mg) were IV injected separately into mice 30 min after bacterial inoculation. Bacterial enumeration was performed using the same protocol.

In vivo survival study. Male CD-1 mice were placed under anaesthesia using a ketamine and xylazine cocktail. They were intratracheally inoculated with 5×10^6 CFU of *P. aeruginosa* and then intratracheally administered with the TAP medium, NP-Cip, 5×10^6 algae-NP(Cip)-robot or 5×10^6 static algae-NP(Cip) at an equivalent Cip amount (500 ng). To compare with the IV treatment, an equivalent Cip amount (500 ng) and clinical dose (1.64 mg) were IV injected separately into mice 30 min after bacterial inoculation. The survival of each mouse was monitored on a daily basis.

In vivo safety studies. Mice were euthanized at 24, 72 and 168 h after the intratracheal administration of TAP medium or 5×10^6 algae-NP(Cip)-robot for sample collection. For the comprehensive metabolic panel and blood cell counts, serum and whole blood were collected. Lab tests were carried out by the University of California San Diego Animal Care Program Diagnostic Services Laboratory. For histological analysis, haematoxylin and eosin staining was performed on the major organs. To evaluate the cytokine levels, BALF was collected by washing the lungs five times using 1 ml of 0.5% (v/v) foetal bovine serum and 2 mM EDTA in PBS through a 23-gauge needle into polytetrafluoroethylene tubing inserted into the trachea. For cytokine analysis, BALF was centrifuged at 700×*g* for 5 min to collect the supernatant. Cytokine concentrations in the BALF were measured in triplicate by a multiplexed sandwich enzyme-linked immunosorbent assay kit (BioLegend). The histology sections of lung tissue were evaluated by the Tissue Technology Shared Resources, University of California San Diego Moores Cancer Center. All the histological assessments were performed in a blinded manner to prevent observer bias.

In vitro cytokine production. J774A.1 macrophage cells were cultured in Dulbecco's modified Eagle medium in a six-well plate at 1×10^6 cells per well. They were subsequently incubated with 5×10^6 algae-NP-robot, 5×10^6 cryo-treated algae-NP-robot, 5×10^6 static algae-NP or 100 ng ml^{-1} flagellin isolated from *Salmonella typhimurium* bacteria (InvivoGen) for 24 h. The cytokine levels were determined by enzyme-linked immunosorbent assay kits (BioLegend).

Reporting summary. Further information on research design is available in the Nature Research Reporting Summary linked to this article.

Data availability

The data supporting the findings of this study are available within the paper, its Supplementary Information files and from the corresponding authors upon reasonable request. Source data are provided with this paper.

References

45. Zhang, Y. et al. A bioadhesive nanoparticle–hydrogel hybrid system for localized antimicrobial drug delivery. *ACS Appl. Mater. Interfaces* **8**, 18367–18374 (2016).
46. Sato, M., Murata, Y., Mizusawa, M., Iwahashi, H. & Oka, S.-I. A simple and rapid dual fluorescence viability assay for microalgae. *Microbiol. Cult. Coll.* **20**, 53–59 (2004).

Acknowledgements

This work is supported by the National Institutes of Health under award no. R01CA200574 (L.Z.).

Author contributions

F.Z., J. Zhuang, L.Z. and J.W. conceived the study and designed the experiments. F.Z., J. Zhuang, Z.L. and H.G. conducted the experiments. F.Z., J. Zhuang, Z.L., H.G., B.E.-F.Á., Y.D., Q.Z., J. Zhou, L.Y., E.K., R.H.F., L.Z. and J.W. analysed the data. F.Z., J. Zhuang, Z.L., H.G., B.E.-F.Á., W.G., V.N., R.H.F., L.Z. and J.W. wrote the manuscript. All the authors reviewed, edited and approved the paper.

Competing interests

The authors declare no competing interests.

Additional information

Supplementary information The online version contains supplementary material available at https://doi.org/10.1038/s41563-022-01360-9.

Correspondence and requests for materials should be addressed to Liangfang Zhang or Joseph Wang.

Peer review information *Nature Materials* thanks Kelly Bachta, Sylvain Martel, Bradley Nelson and the other, anonymous, reviewer(s) for their contribution to the peer review of this work.

Reprints and permissions information is available at www.nature.com/reprints.

nature research

Corresponding author(s): Joseph Wang
Liangfang Zhang

Last updated by author(s): April 20, 2022

Reporting Summary

Nature Research wishes to improve the reproducibility of the work that we publish. This form provides structure for consistency and transparency in reporting. For further information on Nature Research policies, see our Editorial Policies and the Editorial Policy Checklist.

Statistics

For all statistical analyses, confirm that the following items are present in the figure legend, table legend, main text, or Methods section.

n/a	Confirmed	
☐	☒	The exact sample size (*n*) for each experimental group/condition, given as a discrete number and unit of measurement
☐	☒	A statement on whether measurements were taken from distinct samples or whether the same sample was measured repeatedly
☐	☒	The statistical test(s) used AND whether they are one- or two-sided *Only common tests should be described solely by name; describe more complex techniques in the Methods section.*
☐	☒	A description of all covariates tested
☐	☒	A description of any assumptions or corrections, such as tests of normality and adjustment for multiple comparisons
☐	☒	A full description of the statistical parameters including central tendency (e.g. means) or other basic estimates (e.g. regression coefficient) AND variation (e.g. standard deviation) or associated estimates of uncertainty (e.g. confidence intervals)
☒	☐	For null hypothesis testing, the test statistic (e.g. *F*, *t*, *r*) with confidence intervals, effect sizes, degrees of freedom and *P* value noted *Give P values as exact values whenever suitable.*
☒	☐	For Bayesian analysis, information on the choice of priors and Markov chain Monte Carlo settings
☒	☐	For hierarchical and complex designs, identification of the appropriate level for tests and full reporting of outcomes
☒	☐	Estimates of effect sizes (e.g. Cohen's *d*, Pearson's *r*), indicating how they were calculated

Our web collection on statistics for biologists contains articles on many of the points above.

Software and code

Policy information about availability of computer code

Data collection	No standalone or custom software was used.
Data analysis	Software used in analysis include ImageJ, FlowJo 7.6, GraphPad Prism 8, Microsoft Excel.

For manuscripts utilizing custom algorithms or software that are central to the research but not yet described in published literature, software must be made available to editors and reviewers. We strongly encourage code deposition in a community repository (e.g. GitHub). See the Nature Research guidelines for submitting code & software for further information.

Data

Policy information about availability of data

All manuscripts must include a data availability statement. This statement should provide the following information, where applicable:

- Accession codes, unique identifiers, or web links for publicly available datasets
- A list of figures that have associated raw data
- A description of any restrictions on data availability

The datasets are available from the corresponding author on reasonable request.

Field-specific reporting

Please select the one below that is the best fit for your research. If you are not sure, read the appropriate sections before making your selection.

☒ Life sciences ☐ Behavioural & social sciences ☐ Ecological, evolutionary & environmental sciences

For a reference copy of the document with all sections, see nature.com/documents/nr-reporting-summary-flat.pdf

Life sciences study design

All studies must disclose on these points even when the disclosure is negative.

Sample size	No sample size calculation was performed. The in vivo antibacterial efficacy was evaluated with 6 mice per group for bacterial enumeration and with 12 mice per group for survival studies. Sample sizes were determined based on prior experience with the animal model and pilot studies.
Data exclusions	No data were excluded.
Replication	Experiments were repeated and experimental results were reproducible.
Randomization	Samples were randomly allocated to different experimental groups before treatment. Organisms were cultured and maintained in the same environment and randomly allocated to each group.
Blinding	Investigators were not blinded to group allocation during data collection and analysis.

Reporting for specific materials, systems and methods

We require information from authors about some types of materials, experimental systems and methods used in many studies. Here, indicate whether each material, system or method listed is relevant to your study. If you are not sure if a list item applies to your research, read the appropriate section before selecting a response.

Materials & experimental systems

n/a	Involved in the study
☐	☒ Antibodies
☐	☒ Eukaryotic cell lines
☒	☐ Palaeontology and archaeology
☐	☒ Animals and other organisms
☒	☐ Human research participants
☒	☐ Clinical data
☒	☐ Dual use research of concern

Methods

n/a	Involved in the study
☒	☐ ChIP-seq
☐	☒ Flow cytometry
☒	☐ MRI-based neuroimaging

Antibodies

Antibodies used	Pacific Blue-conjugated anti-mouse CD11c (Biolegend, Cat. No. 117322, Clone N418) PE-conjugated anti-mouse Siglec-F (Biolegend, Cat. No. 155505, Clone S17007L) Alexa488 anti-human CD11a (LFA-1) antibody (Biolegend, Cat. No. 301216, Clone HI111)
Validation	Antibodies were validated by the manufacturer and used without further modifications.

Eukaryotic cell lines

Policy information about cell lines

Cell line source(s)	Human neutrophil-like cells (HL-60), murine macrophage cells (J774A.1) and human bronchial epithelial cells (NL-20) were obtained from American Type Culture Collection (CCL-240, TIB-67 and CRL-2503).
Authentication	Cells were used without modification after receiving from the supplier and therefore were not authenticated.
Mycoplasma contamination	The cell line was tested monthly to be negative for mycoplasma contamination.
Commonly misidentified lines (See ICLAC register)	N/A

Animals and other organisms

Policy information about studies involving animals; ARRIVE guidelines recommended for reporting animal research

Laboratory animals	Male CD-1 mice were purchased from Charles River Labs.
Wild animals	N/A
Field-collected samples	N/A
Ethics oversight	All animal experiments were performed in accordance with NIH guidelines and approved by the Institutional Animal Care and Use Committee (IACUC) of University of California, San Diego.

Note that full information on the approval of the study protocol must also be provided in the manuscript.

Flow Cytometry

Plots

Confirm that:

☒ The axis labels state the marker and fluorochrome used (e.g. CD4-FITC).

☒ The axis scales are clearly visible. Include numbers along axes only for bottom left plot of group (a 'group' is an analysis of identical markers).

☒ All plots are contour plots with outliers or pseudocolor plots.

☒ A numerical value for number of cells or percentage (with statistics) is provided.

Methodology

Sample preparation	For flow cytometry analysis of algae-NP-robot, after neutrophil membrane coating onto the DiO-loaded nanoparticles, nanoparticles were conjugated to algae via click chemistry. Details on algae-NP-robot preparation are provided in Methods section. For flow cytometry analysis of algae-NP-robot uptake by alveolar macrophage in vivo, bronchoalveolar lavage fluid was collected from each mouse. RBCs in the mixture were lysed before the cells were blocked with 1% bovine serum albumin and probed with Pacific Blue-conjugated anti-mouse CD11c and PE-conjugated anti-mouse Siglec-F antibodies. Unbound antibodies were washed out with 1% bovine serum albumin prior to analysis. More details are provided in Methods section.
Instrument	Becton Dickinson FACSCanto-II flow cytometer
Software	FlowJo 7.6
Cell population abundance	For algae-NP-robot analysis, 100,000 total events were acquired and for alveolar macrophage analysis, 20,000 cells were collected.
Gating strategy	For algae-NP-robot characterization, preliminary FSC/SSC gates were determined by comparing the population of control sample (i.e. bare algae without modification) with positive algae-NP-robot sample. For algae-NP-robot uptake by alveolar macrophage in vivo, cellular debris were gated out on FSC/SSC plots and doublet exclusion was performed. Specific positive populations were identified by comparing the population with single stained control samples (i.e. cells labeled with only one antibody or algae only).

☒ Tick this box to confirm that a figure exemplifying the gating strategy is provided in the Supplementary Information.